



Plasmonic Nanosensor for Cancer Cell Detection with Multi Fano Resonance

Gaurav Kumar Yadav¹ · Sanjeev Kumar Metya¹

Received: 7 March 2023 / Accepted: 3 April 2023 / Published online: 20 April 2023

© The Author(s), under exclusive licence to Springer Science+Business Media, LLC, part of Springer Nature 2023

Abstract

In the field of biosensing, plasmonics has gained momentum recently as it enables plasmon based circuits to merge two fields of photonics and electronics at nanoscale and also provides the advantage of label-free detection. A Metal Insulator Metal based plasmonic refractive index sensor is conceptualised on panda ring design. Finite Difference Time Domain method is employed to study the transmittance characteristics of the sensor. The transmittance curve exhibits triple Fano Resonances resulting in high sensitivities of 922 nm/RIU, 1730 nm/RIU and 2092.3 nm/RIU for the fano dips at 0.949 μm , 1.728 μm and 2.103 μm respectively. Further investigation is also done with respect to fabrication complexities which may arise using a square slit and its consequent effect on the efficiency of the sensor. The sensor performance is also investigated based on figure of merit which is obtained at a high value of 46.18 RIU⁻¹. The proposed sensor is investigated further for probable detection of cancerous cells namely Jurkat, PC-12, MDA-MB-231, MCF-7 and Basal Cell.

Keywords Fano resonance · Metal insulator metal · Plasmonic sensor · Refractive index sensor · Sensitivity

Introduction

Surface Plasmon Resonance (SPR) [1] has been recently investigated very widely in plasmonics based research. SPR is fundamentally a photonics based quantum electromagnetic phenomenon arising out of interaction of light and free electrons at a metal dielectric interface [2]. SPRs provide a number of advantages which includes real-time and label-free detection, immunity to electromagnetic interference and rapid response time [3]. Plasmonic sensing has emerged as a crucial area of research involving biosensing widely used for sensing traces of biological and chemical molecules [4, 5]. The plasmonic sensor devices are basically based on Metal Insulator Metal (MIM) or Insulator Metal Insulator (IMI) waveguides coupled with cavity resonators [6]. The MIM SPR system provides advantages such as stronger field enhancement, wide range of available frequencies, good properties of light confinement and reduce bending loss [7].

Hence, MIM SPR system becomes one of the best methods in realising nanoscale integrated photonic devices.

Fano Resonance (FR), owing to its useful properties has been exploited in plasmonic sensing applications [8]. The independent tunability of the FRs helps in achieving demands in application with convenience through easy manipulation. Hence, it is efficiently used in chemical and biosensing applications. A great use of plasmonics is in the excitation of the FR, it is achieved via the interaction of the dark and bright mode of the radiative spectrum [9]. A distinctive feature of the FR which makes it attractive in the sensing application is the high value of the quality factor which enhances the photon lifetime in the resonator hence enabling a longer light matter interaction [10, 11]. FR differs from the Lorentzian curve as the FR based systems exhibit asymmetrical profile.

Finite Difference Time domain (FDTD) method [12] is employed, a method used to solve electromagnetic problems having time dependencies. It solves Maxwell's equations on a mesh and computes 'E' and 'H' at grid points. FDTD has advantages over similar methods available for time dependent problem solving, such as Finite Element Method (FEM) [13]. The main advantage of FDTD over FEM is that, unlike FEM, which only addresses uncoupled harmonic issues, FDTD's time dependence is transient or pulsed and can be converted into frequency domain problems.

✉ Sanjeev Kumar Metya
smetya@gmail.com

Gaurav Kumar Yadav
gauravyadav7ece@gmail.com

¹ Department of Electronics and Communication Engineering,
National Institute of Technology Arunachal Pradesh,
Jote 791113, Arunachal Pradesh, India

Recently a plasmonic based sensor has been reported by [14] for virus detection based on tuned light metamaterial absorber; however, apart from the complex design, the sensitivity of the virus sensor is on the lower side of 76 nm/RIU; moreover, only a comparative analysis has been done based on structure dimension with respect to the reported sensors without mentioning the FOM. [15] proposed a sensor for biological and chemical sensing based on gold nano array with a FOM of 98 RIU^{-1} ; however, the highest sensitivity obtained is still on the lower side with a value of 880 nm/RIU. A bowtie cavity based glucose sensor is reported by [16] with sensitivity of 1500 nm/RIU and highest FOM of 50 RIU^{-1} ; however, the design complexities may pose an issue with regard to fabrication. [17] proposed a temperature sensor based on ring encapsulated circular cavity with a FOM of 18.74 RIU^{-1} and sensitivity of 1350 nm/RIU which is still on the lower side compared to the already reported sensors. [18] proposed a sensor based on gold plasmonic square nanohole arrays deposited on a silicon dioxide substrate with a sensitivity of 944 nm/RIU and a FOM of 15.25 without mentioning any specific applications. The structure becomes complex due to the presence of nanohole arrays which might lead to fabrication issues. [19] reported a sensor based on slot cavity resonant system with a sensitivity of 1000 nm/RIU and a FOM of $\sim 38 \text{ dB}$ at 890 nm. The authors proposed the applicability of the structure for not only refractive index sensing but also in the fast/slow light region. The structure might have fabrication issues due to the presence of multiple slots as well as the lower sensitivity fails to justify the complexity of the structure. [20] proposed a sensor based on a four-step stub waveguide; however, its reported sensitivity of 1078 nm/RIU still falls on the lower side with FOM* value of 1.54×10^{-6} without any specific applications. [21] designed a microsensors based on whistle shaped cavity with a sensitivity of 1229 nm/RIU without mentioning FOM and applications, the design becomes a bit complicated for practical applications.

Fig. 1 Schematic of the proposed sensor; R = Radius of the central ring, r = Radius of the adjacent ring

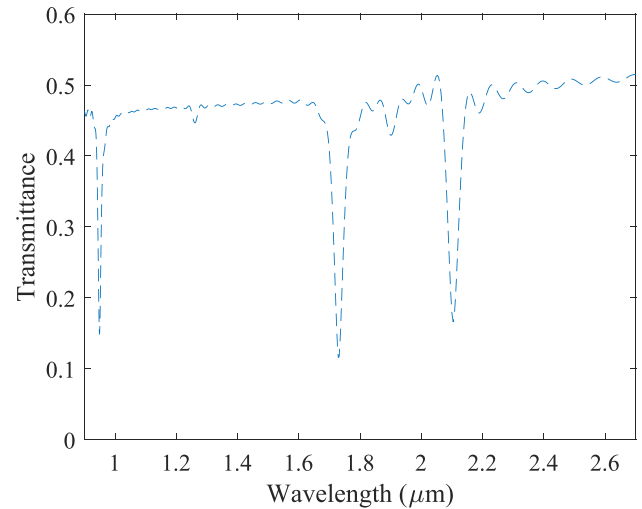
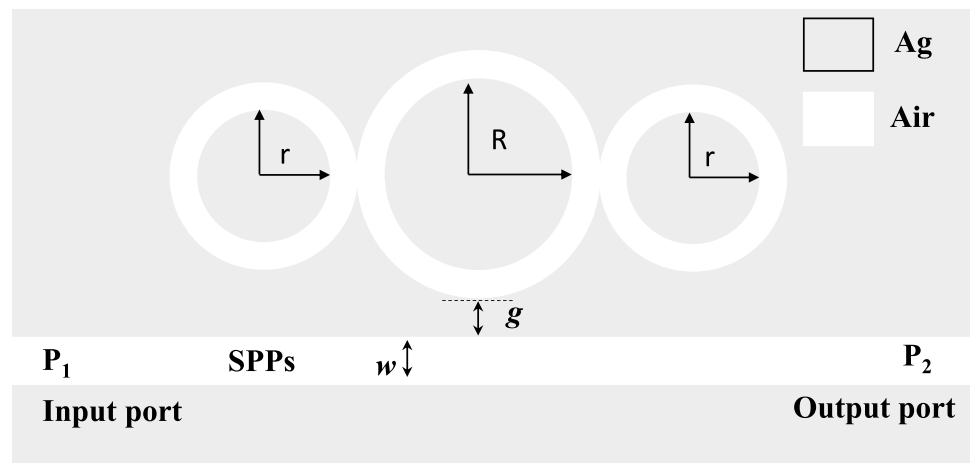


Fig. 2 Transmittance based on waveguide configuration

In this paper we proposed a plasmonic refractive index sensor based on MIM SPR system with panda ring resonators. FDTD has been used to study the transmittance characteristics of the device along with Perfect Matched Layer (PML) boundary condition. The transmission characteristics exhibit multiple FRs and investigation is also done for biosensing applications. The organisation of the paper is as follows: the ‘[Theoretical Model and Structure of the Proposed Sensor](#)’ section provides detailed description about the theoretical background of the proposed design as well as explains the structural parameters followed by the ‘[Results and Discussions](#)’ section explaining the results and includes discussion on potential fabrication issues along with sensitivity and a comparative analysis with the existing sensors. The ‘[Application Prospects](#)’ section explains the biosensing application prospects of the proposed design and finally the ‘[Conclusion](#)’ section concludes the paper.

Theoretical Model and Structure of the Proposed Sensor

Figure 1 illustrates the schematic of the proposed sensor, the structure consists of a MIM waveguide coupled with a panda ring resonator. The width ‘w’ for all the waveguides is fixed at $w = 50$ nm to ensure the availability of single fundamental transverse mode (TM). The radius of the central ring is kept at $R = 180$ nm and the radius of the two adjacent rings is kept at $r = 113$ nm. The separation between the linear waveguide and the panda ring resonator is kept at $g = 10$ nm. The total length and width of the structure under simulation is $2.8 \mu\text{m}$ and $1.5 \mu\text{m}$ respectively, which is smaller in compared to [22]. Silver (Ag) is used as the metallic component of the MIM waveguide because compared to other noble metals it has better optical properties. The dispersive metal property is defined using the Lorentz dispersive model which explains the frequency dependency of the dielectric permittivity [23]. The fundamental TM mode is excited using the dispersion relation [24]:

$$\epsilon_d \kappa_m + \epsilon_m \kappa_d \tanh\left(\frac{\kappa_d w}{2}\right) = 0 \tag{1}$$

where κ_m and κ_d are defined as: $\kappa_m = \sqrt{\beta^2 - \epsilon_m \kappa_o^2}$ and $\kappa_d = \sqrt{\beta^2 - \epsilon_d \kappa_o^2}$, ϵ_d and ϵ_m are the dielectric constants of insulator and metal respectively, $\kappa_o = \frac{2\pi}{\lambda_o}$ is the wave vector of light where λ_o is the wavelength in free space, β denotes the propagation constant of the SPPs.

The incident light traversing along the waveguide gets coupled in the panda ring resonator creating a phase difference which is represented as [25]:

$$\Delta\phi = \frac{2\pi}{\lambda_o} n_{eff} L + \phi_{ref} \tag{2}$$

where L is the effective length of the resonators, ϕ_{ref} represents the metal insulator interface phase shift and $n_{eff} = \frac{\beta}{\kappa_o}$ represents the effective refractive index of the waveguide. The waves resonate in the cavity when $\Delta\phi = 2\pi m$ ($m = 1, 2, 3, \dots$) and the resulting resonant wavelength is represented as [26]:

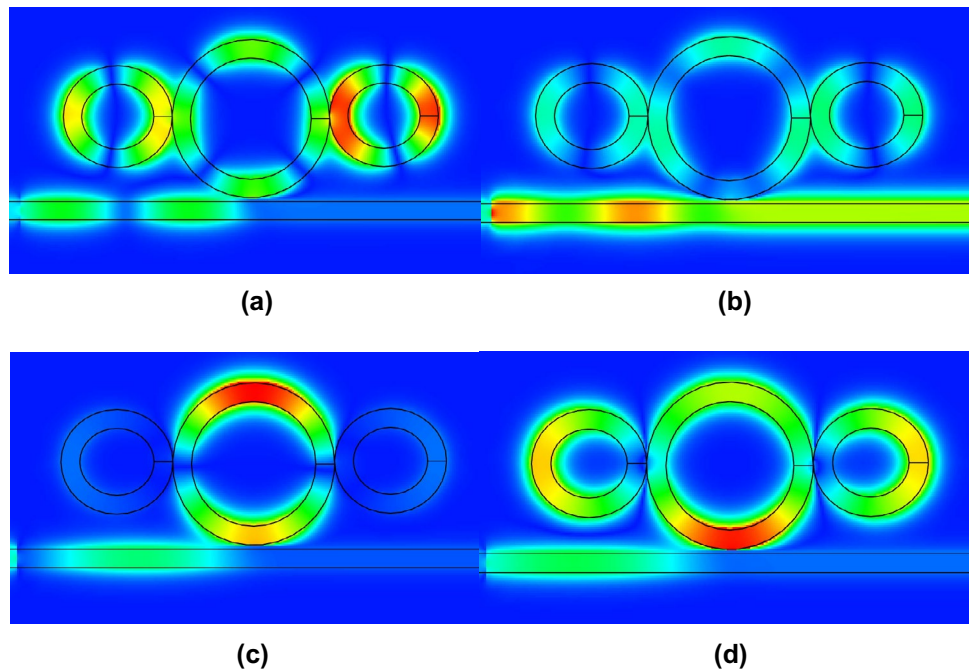
$$\lambda_{res} = \frac{n_{eff} L}{m - \frac{\phi_{ref}}{2\pi}} \tag{3}$$

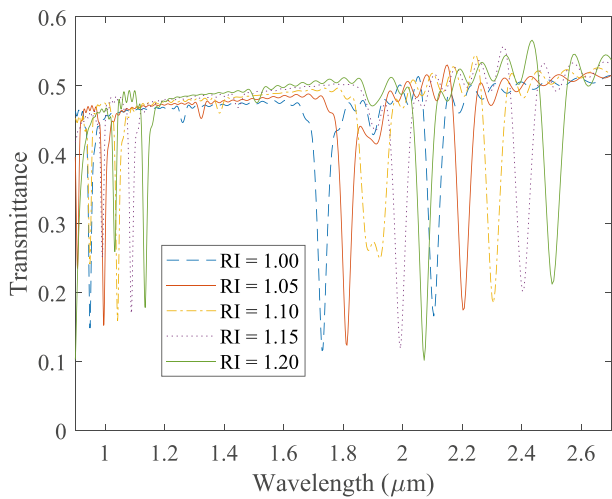
This equation implies that λ_{res} is directly proportional to L (effective length of the resonators) and n_{eff} . Furthermore, the Multimode Interference Couple Mode Theory (MICMT) can be used to explain the transmittance characteristics of the coupled resonators and the relation between the resonators is given as [27]:

$$\frac{da_m}{dt} = \left(-j\omega_m - \frac{1}{\tau_{m,in}} - \frac{1}{\tau_{m,1}} - \frac{1}{\tau_{m,2}}\right) a_m + k_{m1} S_{m1} + k_{m2} S_{m2} \tag{4}$$

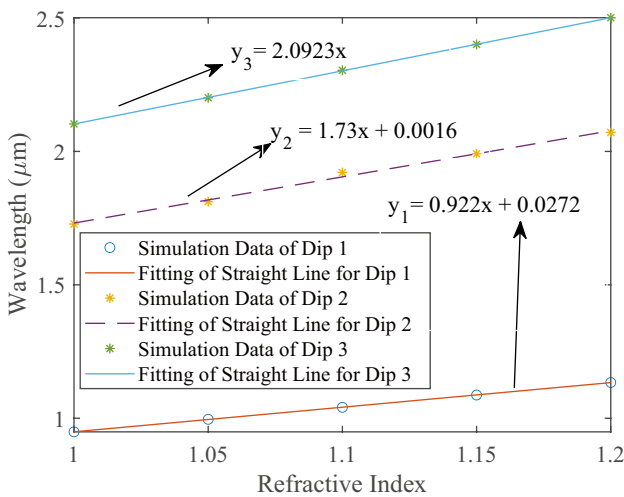
where ω_m and a_m represents the resonant frequency and normalised amplitude of the m^{th} resonant mode, $\tau_{m,in}$ represents the decay time of internal loss of m^{th} resonant mode, $\tau_{m,1}$ and $\tau_{m,2}$ are the decay time of the coupling between the

Fig. 3 Magnetic field profile $|Hz|^2$ at wavelength **a** $\lambda = 0.949 \mu\text{m}$ **b** $\lambda = 0.980 \mu\text{m}$ **c** $\lambda = 1.728 \mu\text{m}$. **d** $\lambda = 2.103 \mu\text{m}$





(a)



(b)

Fig. 4 a Transmittance obtained for different RI. Relationship between the resonant wavelength with respect to RI for b FR₁ and FR₂ and FR₃

resonators and the waveguides, k_{m1} and k_{m2} are the coupling coefficients connoting the coupling of m^{th} mode between the resonating structure and the waveguide [28].

$$S_{1-} = -S_{1+} + \sum_m k_{m1} a_m e^{j\phi_{m,1}} \tag{5}$$

$$S_{2-} = -S_{2+} + \sum_m k_{m2} a_m e^{j\phi_{m,2}} \tag{6}$$

Normalised amplitude at the input and output of MIM waveguides is denoted by $S_{1,2+}$ and $S_{1,2-}$ respectively and + and – are used to signify the incoming or outgoing signal; $\phi_{m,1}$ and $\phi_{m,2}$ are the coupling phases of m^{th} resonant modes. Considering ϕ_m to be the m^{th} mode phase, the transmittance thus can be represented as [29]:

$$T = \left| \frac{S_{2-}}{S_{1+}} \right|^2 = \left| \sum \frac{2e^{j\phi_m}}{-j(\omega - \omega_m)\tau_m + 2 + \frac{\tau}{\tau_{m,in}}} \right|^2 \tag{7}$$

Results and Discussions

Using a two-dimensional FDTD method, the proposed sensor’s transmission characteristics are investigated. The boundary condition in effect across the sensor is the Perfect Matched Layer (PML) to minimise simulation errors and reflections from the side walls. SPPs can be excited at the metal insulator interface when the TM polarised light is incident to the rectangular waveguide. The investigation of the transmission spectrum is done with the help of power that is normalised for a p-polarised light with the input at the output. Figure 2 represents the transmission characteristics of the proposed sensor consisting of a rectangular waveguide coupled with a panda ring resonator in a MIM setup. In Fig. 2 the asymmetric dips are apparent, this behaviour of the graph can be attributed to Eq. (3).

In Fig. 2 it can be visualised in the transmission characteristics that three fano profiles are obtained with dips at $\lambda = 0.949 \mu\text{m}$ (FR₁), $\lambda = 1.728 \mu\text{m}$ (FR₂) and $\lambda = 2.103 \mu\text{m}$ (FR₃) respectively. As per Eqs. (4–7), the SPPs are injected in the MIM waveguide through the input port, hence S_{2+} becomes zero. When the input and output waveguides are identical and are symmetrically distributed on both sides of the cavity resonators then $\tau_m = \tau_{m1} = \tau_{m2} = \tau_{m3}$, where τ_m is the algebraic value replacing τ_{m1} , τ_{m2} and τ_{m3} . Also the coupling phase becomes equal to the phase difference between the resonators. Considering ϕ_m to be the m^{th} mode phase, $\phi_m = \phi_{m1} + \Delta\phi_m$ where $\Delta\phi_m$ denotes the phase difference between input and output port. In relation to the transmittance curve obtained in Fig. 2 the above approximations compliments the FDTD methodology used.

Further, to understand the fundamental nature of the transmission spectrum FR magnetic profile is investigated as shown in Fig. 3. All field profiles have been normalised for better understanding. In Fig. 3b it is observed that SPPs pass through the linear rectangular waveguide despite of significant coupling in the panda ring resonators. Whereas, in Fig. 3a, c and d it can be observed that very little or no magnetic field is obtained at the output as the coupling in the panda ring resonators is very significant leading to destructive interference between the linear waveguide and the panda ring resonators. Hence, in Fig. 2 dips in the transmittance curve are observed which are asymmetric in nature. The asymmetric profile of the resonance is called as Fano Resonance (FR). These FRs helps in realisation of optical sensors via their consequent

shifts in the transmittance graph. The application of FRs in sensing is enhanced due to the presence of multiple FRs. These multiple FRs help in better utilisation of light energy and they exist due to the presence of a number of discrete states born out of interaction between different resonating structures.

To better understand the performance of the device the effect of Refractive Index (RI) is investigated. In Fig. 4a a plot of transmittance curve can be seen with respect to RI. The RI is varied from 1.00 to 1.20 with a step size of 0.05. The variation in RI is tested in the panda ring resonant cavity, using ring resonators provides an additional advantage that the sensing can be tested for a small volume of sample specimen. A redshift is observed in Fig. 4a in the resonant wavelength with respect to variation in the RI. In Fig. 4b a linear relationship between wavelength and RI can be observed for FR₁, FR₂ and FR₃. The linear coefficients of FR₁, FR₂ and FR₃ are obtained as 0.999, 0.995 and 0.999 respectively, which signifies a good performance. Spectral sensitivity is an important parameter to judge the performance of the sensor, mathematically it is represented as $S = \frac{\Delta\lambda}{\Delta n}$ where $\Delta\lambda$ is the redshift in the resonant wavelength and Δn is the change in RI. From Fig. 4a the spectral

sensitivity is found as 922 nm/RIU, 1730 nm/RIU and 2092.3 nm/RIU at FR₁, FR₂ and FR₃ respectively. Thus, it is observed that FR₃ has a superior spectral sensitivity for RI sensing compared to FR₁ and FR₂.

Investigation is also done for fabrication issues arising out of deviation from the optimised structure. The investigation is done with respect to improper etching process represented using slits at different positions on the panda ring resonator as shown in Fig. 5a, b and c respectively. The effect on the transmittance of the sensor due to the presence of the slits can be observed in Fig. 5d and its consequent effect on the sensitivity can be seen in Fig. 5e. The sensitivity is investigated for FR₃ only as it exhibits the highest value. As shown in Fig. 5a, b and c the slits are placed in three different configurations along the panda ring. When a single slit is introduced only in the central ring a decrease in the sensitivity by a value of 75 nm/RIU from the peak value is observed irrespective of the width and position of the slit. Similarly, when slits are introduced in the outer two rings and all the three rings a significant decrease of 109 nm/RIU and 107 nm/RIU from the peak value is observed in the sensitivity compared to the optimised design. These variations can be understood from Fig. 5d, it is evident from the graph

Fig. 5 a, b and c Different positions of slits d Effect on transmittance due to the introduction of slits e Relationship between the resonant wavelength with respect to RI depending on the position of the slit

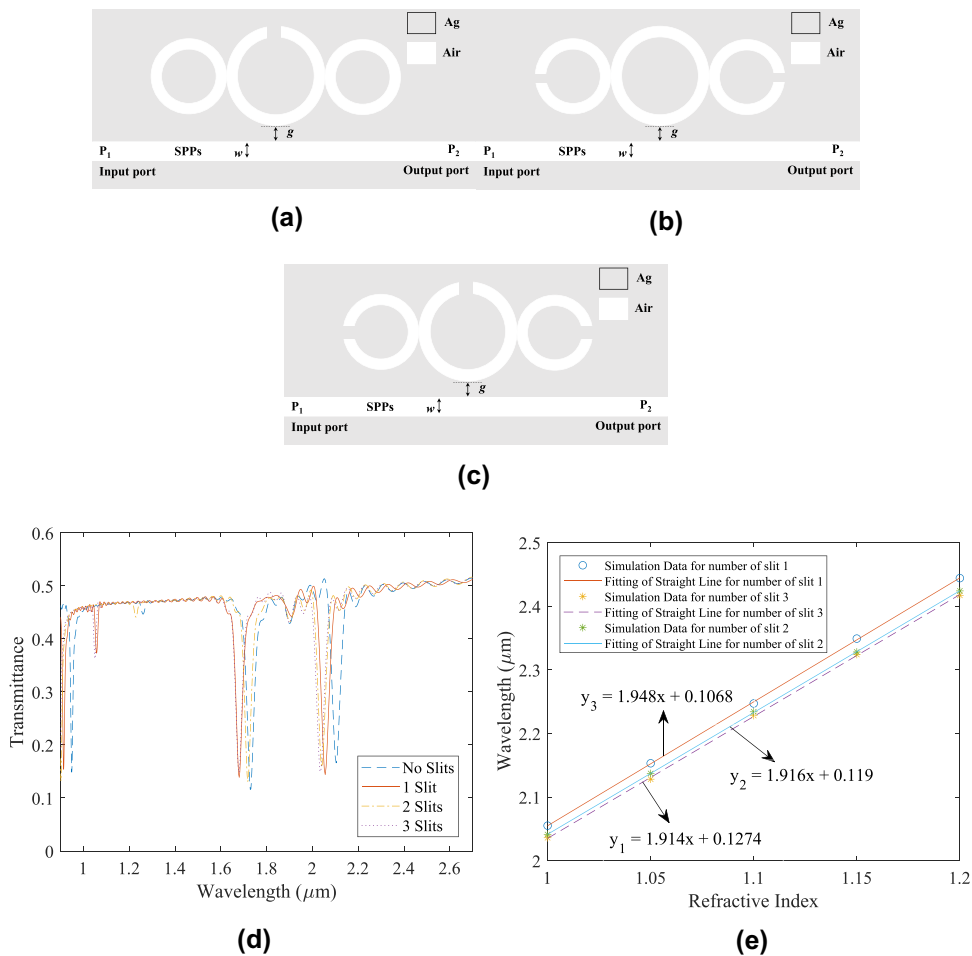


Table 1 Comparative analysis of sensors based on different structures

Structure	Reference	Sensitivity (nm/RIU)	FOM (RIU ⁻¹)
Cross shaped resonator system	[33]	795	-
Semi circular cavity system	[34]	579	12.46
Quantum and nano dots	[35]	1434.5	35.86
Stub and ring resonator	[36]	1650	117.8
H shaped resonator	[37]	1007.78	29
Panda ring resonator	Proposed device	2092.3	46.18

that as slits are introduced in the structure a blue shift can be observed with increase in the number of slits. This blueshift occurs due to the interruption in the otherwise continuous coupling inside the panda ring due to the presence of the slit, hence resulting in consequent decrease in the sensitivity of the sensor. Hence, the potential effect of improper etching process can be deduced based on the above results.

Additionally, Figure of Merit (FOM) is also factored in to investigate the performance of the sensor, it is represented as [30]:

$$FOM = \max \left(\left| \frac{dT(\lambda)}{dn(\lambda)T(\lambda)} \right| \right) \quad (8)$$

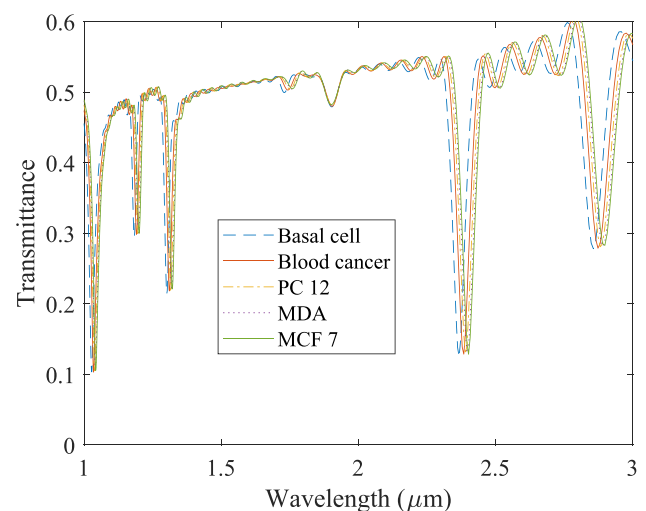
where $T(\lambda)$ is the transmittance at a particular wavelength and $\frac{dT(\lambda)}{dn(\lambda)}$ is the change in transmittance at a fixed wavelength induced by the change in refractive index. The FOM of the structure is analysed for a change in refractive index varying from 1 to 1.1, and the consequent change in resonant wavelength at the dip of the transmittance curve results in a shift from 2103 nm to 2304 nm, based on Eq. (8), a high FOM of 955.7 RIU⁻¹ is achieved. This FOM is generally termed as FOM* [31]. FOM is also calculated using the conventional formula, i.e. $FOM = \frac{S}{FWHM}$ and is found to be 46.18 RIU⁻¹, where S is the sensitivity of the sensor and FWHM is the Full Width Half Maxima [32] of the FR₃.

A comparative analysis of different plasmonic sensors as described in [32, 34–37] along with the proposed device is shown in Table 1. It is evident from Table 1 that compared to [33] the performance parameters of the proposed sensor is much better in terms of sensitivity of the reported sensor. In [34] the reported sensor has a lower sensitivity as well as lower FOM compared to the proposed sensor. The spectral sensitivity is the most important parameter for a RI sensor, in [35] not only the FOM achieved is lower but also the sensitivity obtained is comparatively lower than the proposed sensor. In [36] although the FOM obtained is higher but the spectral sensitivity is still lower than the proposed design. In [37] it can be seen that in comparison to the proposed sensor the FOM and sensitivity of the reported sensor is lower. There is a minimum trade-off between the complexity of the structure and the performance parameters for the proposed sensor. A

relatively higher value of FOM is produced as a result of the presence of a sharp and narrow FWHM asymmetric Fano Resonance profile. All these significant properties of the proposed device helps us to consider it as a contender for on-chip optical sensor applications. On-chip optical sensing is made possible by the proposed sensor's high sensitivity and FOM with triple Fano Resonance profile.

Application Prospects

The sensing application is investigated for the detection of five different cells effected by cancer. The cells that are considered for investigation are Jurkat, PC-12, MDA-MB-231, MCF-7 and Basal Cell [38]. The refractive index of the cancer infected cells of the aforementioned cells are 1.39, 1.395, 1.399, 1.401 and 1.38 respectively [39]. The analyte consisting of the cancer cells under investigation is introduced in the panda ring cavity. A redshift is observed in the transmittance curve with respect to RI of the cancer cells as evident from Fig. 6. It can be visualised that the resonant wavelength is shifting with the variation of RI. Fabrication of the device can be done using Electron-beam lithography or nano-imprint lithograph [40].

**Fig. 6** Transmittance obtained for different concentration of analyte

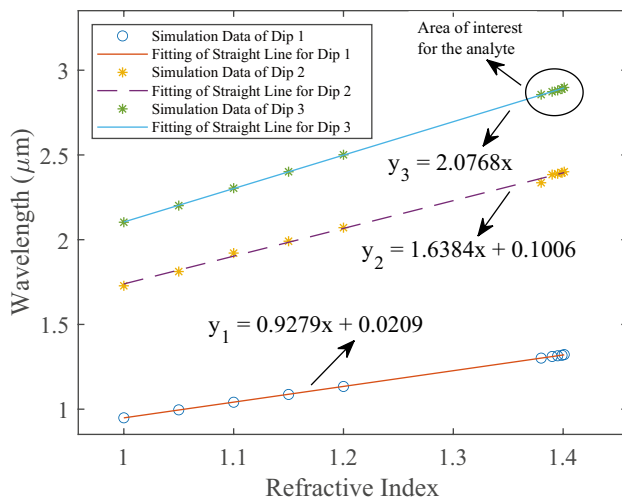


Fig. 7 Fitting line of sensitivity for the analyte at respective FR dips

Cavity attraction method can be used to introduce the material under test into the cavity [41]. In Fig. 7 a linear relationship between the resonant wavelength and RI is obtained with linear coefficients of 1, 0.998 and 1 respectively which denotes towards a good performance. The circled area in Fig. 7 represents the area of interest for sensing at FR_3 . The same area of interest can also be used for detection at FR_1 and FR_2 but with a reduced sensitivity compared to FR_3 .

Conclusion

A plasmonic MIM waveguide setup consisting of linear rectangular waveguide coupled with panda ring resonator is proposed and its transmission characteristics is investigated. The transmission characteristics exhibits three Fano resonances at 0.949 μm , 1.728 μm and 2.103 μm respectively. Sensitivity and FOM are used to examine the proposed sensor's performance, which are both obtained at high levels of 2092 nm/RIU and 46.18 RIU⁻¹ respectively. To identify the potential fabrication issues the proposed design is further investigated by introducing different number of slits. Moreover, the biosensing application is also investigated using five different types of cancerous cells. The transmittance curve shows a visible redshift and the sensitivity graph exhibits a linear relationship between the resonant wavelength and RI. Highest sensitivity of 2076.8 nm/RIU for the cancer cell detection is obtained, which nearly matches the performance of the proposed sensor. Hence, the bio-analyte sensing potential of the proposed sensor is investigated.

Author Contributions Gaurav Kumar Yadav: conceptualisation, device design, simulation and analysis, manuscript preparation. Sanjeev Kumar Metya: manuscript finalisation and supervision.

Data Availability The authors confirm that all data are included within the manuscript.

Declarations

Ethics Approval Not applicable

Consent to Participate Not applicable

Consent for Publication We are hereby giving our consent to Springer Nature for publication of this work.

Conflict of Interest The authors declare no competing interests.

References

- Vajdi A, Sadeghi M, Adelpour Z (2022) Tunable and sensitive graphene-plasmonic opto-fluidic nano sensor. *Opt Quant Electron* 54(3):188
- Zalevsky Z, Abdulhalim I (2010) Chapter 6 - plasmonics. In: Zalevsky Z, Abdulhalim I (eds) *Integrated Nanophotonic Devices. Micro and Nano Technologies*, William Andrew Publishing, Oxford, pp 175–240
- Harhouz A, Hocini A (2021) Highly sensitive plasmonic temperature sensor based on Fano resonances in MIM waveguide coupled with defective oval resonator. *Opt Quant Electron* 53(8):439
- Goyal AK, Pal S (2020) Design analysis of Bloch surface wave based sensor for haemoglobin concentration measurement. *Appl Nanosci* 10:3639–3647
- Goyal AK, Saini J (2020) Performance analysis of Bloch surface wave-based sensor using transition metal dichalcogenides. *Appl Nanosci* 10:4307–4313
- Hocini A, Ben Salah H, Khedrouche D, Melouki N (2020) A high-sensitive sensor and band-stop filter based on intersected double ring resonators in metal-insulator-metal structure. *Opt Quant Electron* 52:1–10
- Hocini A, Ben Salah H, Temmar MNe (2021) Ultra-high-sensitive sensor based on a metal-insulator-metal waveguide coupled with cross cavity. *J Comput Electron* 20(3):1354–1362
- Cao G, Dong S, Zhou LM, Zhang Q, Deng Y, Wang C, Zhang H, Chen Y, Qiu CW, Liu X (2020) Fano resonance in artificial photonic molecules. *Advanced Optical Materials* 8(10):1902153
- Zafar R, Nawaz S, Singh G et al (2018) Plasmonics-based refractive index sensor for detection of hemoglobin concentration. *IEEE Sens J* 18(11):4372–4377
- He J, Yang S (2016) Line shapes in a plasmonic waveguide system based on plasmon-induced transparency and its application in nanosensor. *Opt Commun* 381:163–168
- Sharma Y, Zafar R, Metya SK, Kanungo V (2020) Split ring resonators-based plasmonics sensor with dual fano resonances. *IEEE Sens J* 21(5):6050–6055
- Nair SK, Shinoj V (2021) Enhanced absorption in thin film silicon solar cell using plasmonic nanoparticles: An FDTD study. In: *AIP Conference Proceedings*, AIP Publishing LLC, vol 2336, p 020003
- Reddy JN (2019) *Introduction to the Finite Element Method*, 4th edn. McGraw-Hill Education, New York
- Vafapour Z, Ghahraloud H, Keshavarz A, Islam MS, Rashidi A, Dutta M, Stroschio MA (2021) The potential of refractive index nanobiosensing using a multi-band optically tuned perfect light metamaterial absorber. *IEEE Sens J* 21(12):13786–13793
- Chen H, Wang X, Zhang J, Rao X, Yang H, Qi Y, Tang C (2023) Theoretical study of surface plasmonic refractive index sensing

- based on gold nano-cross array and gold nanofilm. *Physica B* 655:414746
16. Chou Chau YF (2021) Multiple-mode bowtie cavities for refractive index and glucose sensors working in visible and near-infrared wavelength ranges. *Plasmonics* 16(5):1633–1644
 17. Butt MA, Khonina SN, Kazanskiy NL (2022) Simple and improved plasmonic sensor configuration established on MIM waveguide for enhanced sensing performance. *Plasmonics* 17(3):1305–1314
 18. Shafiq R, Iqbal J, Khan AD, Rehman AU (2022) A theoretical study of broadband extraordinary optical transmission in gold plasmonic square nanohole arrays and its application on refractive index sensor. *Opt Quant Electron* 54(3):156
 19. Guo Z, Wen K, Qin Y, Fang Y, Li Z, Chen L (2022) A Plasmonic Refractive-Index Sensor Based Multiple Fano Resonance Multiplexing in Slot-Cavity Resonant System. *Photonic Sensors* 12(2):175–184
 20. Najjari V, Mirzanejad S, Ghadi A (2022) Plasmonic refractive index sensor and plasmonic bandpass filter including graded 4-step waveguide based on Fano resonances. *Plasmonics* 17(4):1809–1817
 21. Li B, Sun H, Zhang H, Li Y, Zang J, Cao X, Zhu X, Zhao X, Zhang Z (2022) Refractive index sensor based on the fano resonance in metal-insulator-metal waveguides coupled with a whistle-shaped cavity. *Micromachines* 13(10):1592
 22. Wang Y, Hou ZL, Yu L (2021) Plasmonic nanosensor based on sharp fano resonances induced by aperture-coupled slot system. *Opt Commun* 480:126438
 23. Li J, Chen J, Liu X, Tian H, Wang J, Cui J, Rohimah S (2021) Optical sensing based on multimode fano resonances in metal-insulator-metal waveguide systems with x-shaped resonant cavities. *Appl Opt* 60(18):5312–5319
 24. Zhang Y, Cui M (2019) Refractive index sensor based on the symmetric MIM waveguide structure. *J Electron Mater* 48:1005–1010
 25. Li Z, Wen K, Chen L, Lei L, Zhou J, Zhou D, Fang Y, Wu B (2019) Refractive index sensor based on multiple Fano resonances in a plasmonic MIM structure. *Appl Opt* 58(18):4878–4883
 26. Al Mahmud R, Faruque MO, Sagor RH (2021b) Plasmonic refractive index sensor based on ring-type pentagonal resonator with high sensitivity. *Plasmonics* 16:873–880
 27. Chen Y, Luo P, Liu X, Di Y, Han S, Cui X, He L (2018) Sensing performance analysis on Fano resonance of metallic double-baffle contained MDM waveguide coupled ring resonator. *Opt Laser Technol* 101:273–278
 28. Yu S, Su Y, Sun Z, Zhao T, Yu J (2021) Multi-Fano resonances in MIM waveguides coupled with split annular cavity connected with rectangular resonator and application for multichannel refractive index sensor. *J Nanophotonics* 15(1):016004
 29. Asgari S, Pooretamad S, Granpayeh N (2020) Plasmonic refractive index sensor based on a double concentric square ring resonator and stubs. *Photonics Nanostruct Fundam Appl* 42:100857
 30. Liu X, Yang Q, Peng K, Zhang B, Bai H, Li X, Tan Y, Zhang Z, Guo F (2021) Tunable triple fano resonance in mim waveguide system with split ring resonator. *Opt Quant Electron* 53:1–12
 31. Chen Y, Chen L, Wen K, Hu Y, Lin W (2020) Independently tunable Fano resonances in a metal-insulator-metal coupled cavities system. *Appl Opt* 59(5):1484–1490
 32. Qi YP, Wang LY, Zhang Y, Zhang T, Zhang BH, Deng XY, Wang XX (2020) Multiple fano resonances in metal-insulator-metal waveguide with umbrella resonator coupled with metal baffle for refractive index sensing. *Chin Phys B* 29(6):067303
 33. Su C, Zhu J (2021) Novel SPR sensor based on MIM-based waveguide and an asymmetric cross-shaped resonator. *Plasmonics* 16(3):769–775
 34. Tavana S, Bahadori-Haghighi S (2022) Visible-range double fano resonance metal-insulator-metal plasmonic waveguide for optical refractive index sensing. *Plasmonics* 17(6):2441–2449
 35. Sasi S, Francis SM, Jacob J, Thomas VI (2021) A tunable plasmonic refractive index sensor with ultrabroad sensing range for cancer detection. *Plasmonics* 16(5):1705–1717
 36. Zhou C, Huo Y, Guo Y, Niu Q (2021) Tunable multiple fano resonances and stable plasmonic band-stop filter based on a metal-insulator-metal waveguide. *Plasmonics* 16(5):1735–1743
 37. Adhikari R, Sbeah Z, Gupta R, Chauhan D, Nunzi JM, Prakash Dwivedi R (2022) Compact and sensitive H-Shaped metal-dielectric-metal waveguide plasmonic sensor. *Plasmonics* 17(4):1593–1606
 38. Parvin T, Ahmed K, Alatwi AM, Rashed ANZ (2021) Differential optical absorption spectroscopy-based refractive index sensor for cancer cell detection. *Opt Rev* 28:134–143
 39. Al Mahmud R, Faruque MO, Sagor RH (2021a) A highly sensitive plasmonic refractive index sensor based on triangular resonator. *Opt Commun* 483:126634
 40. Amoosoltani N, Yasrebi N, Farmani A, Zarifkar A (2020) A plasmonic nano-biosensor based on two consecutive disk resonators and unidirectional reflectionless propagation effect. *IEEE Sens J* 20(16):9097–9104
 41. Zhang W, Yang S, Jiang M, Hu Y, Hu C, Zhang X, Jin Z (2021) Nanocapillarity and nanoconfinement effects of pipet-like bismuth@ carbon nanotubes for highly efficient electrocatalytic CO₂ reduction. *Nano Lett* 21(6):2650–2657

Publisher's Note Springer Nature remains neutral with regard to jurisdictional claims in published maps and institutional affiliations.

Springer Nature or its licensor (e.g. a society or other partner) holds exclusive rights to this article under a publishing agreement with the author(s) or other rightsholder(s); author self-archiving of the accepted manuscript version of this article is solely governed by the terms of such publishing agreement and applicable law.